



## A Structural and Electrical characterizations of new synthesized PVA/ PoPDA-rGO-ZnO Nano composite

Zamn R. Ali and Amir F. Dawood\*



CrossMark

*<sup>a</sup>Department of Chemistry, College of Science, University of Diyala*

### Abstract

Control of dielectric properties of PVA/PoPDA-rGO-ZnO polymeric composites is an important issue in electrical applications. As a flexible dielectric nanocomposite for enhancing electrical energy storage (Capacitors) and electrical conductivity of the polymer. The synthesis of the crystalline structure of PVA/PoPDA-rGO-ZnO nanocomposite is achieved using several facile preparation methods. The study of structural properties is achieved by x-ray diffraction (XRD), scanning electron microscopy (SEM), and Fourier-transform infrared (FT-IR), while the electrical properties are characterized using capacitance data in the frequency range (1 MHz to 5 MHz) under the application of an alternating electrical field. The XRD, SEM, and FT-IR show the formation of the crystalline phase PVA/PoPDA-rGO-ZnO nanocomposite. The capacitance data test at the different frequencies indicated good electrical properties of the ternary nanocomposite. The PVA/PoPDA-rGO-ZnO achieved the highest A.C. electrical conductivity ( $\sigma_{ac}$ ) and dielectric constant ( $\epsilon'$ ) ( $3.74 \times 10^{-5}$  S/m), (1.7645) at frequencies of (5 MHz), (1 MHz) respectively, while the lowest dissipation factor ( $\epsilon''$ ) (0.29054) at the frequency of (5 MHz). The rGO nanosheets and ZnO nanoparticles, which look like flowers, play an effective role in the electrical properties. The rGO nanosheets within the PVA film act as a network of nanocapacitors to store the electric charges. The results proved that the electrical properties strongly depend on the applied electric field frequency.

Keywords: Nanostructures, rGO nanosheets, ZnO nanoparticles, Ternary nanocomposite, Structural and electrical characterizations.

### 1. Introduction

In recent years, materials based on carbon, including graphene oxide GO, reduced graphene oxide rGO, carbon nanotubes, and their nanocomposites, have attracted more attention due to their interesting mechanical, chemical, and electrical properties. The materials composed of reduced graphene oxides rGO and zinc oxide ZnO have presented attractive performance with high sensitivity, short-time response, and applicability to electronic devices such as photocatalytic, capacitors and sensors [1,2,3,4]. On the other hand, good conductive polymers have also attracted great interest due to their wide application in flexible electronic devices. These conductive polymers have several advantages, including low-cost, simple to fabricate, flexible, and stable structure over time [5]. The conductive polymers have superior conductivity and a large surface area that effectively

improves the humidity performance and gas sensing of electronic devices manufactured using these conductive polymers [6]. Many conductive polymers and their nanocomposites have been applied in flexible capacitors, sensors, rechargeable batteries, microelectronics electrocatalysts, devices, such as polythiophene, polyaniline, polypyrrole, and other polymers. Among these conductive polymers, poly (o-phenylenediamine) (PoPDA) and its nanocomposites such as I<sub>2</sub>/PoPDA, Cu/PoPDA, Fe/PoPDA, Zn/NiO, and GO-TiO<sub>2</sub>/PoPDA nanocomposite have been used to improve the electrical and optical properties [7,8]. Poly (o-phenylenediamine) (PoPDA) is a polyaniline derivative formed by the substitution of hydrogens with amino groups. PoPDA polymerizes easily at room temperature or at 100 °C using chemical oxidants. Both redox and conductive polymer properties. The PoPDA changes from benzenoid to

\*Corresponding author e-mail: [zamnrivadh437@gmail.com](mailto:zamnrivadh437@gmail.com); (Zamn R. Ali).

Receive Date: 16 August 2021, Revise Date: 03 October 2021, Accept Date: 17 October 2021

DOI: 10.21608/EJCHEM.2021.91060.4331

©2022 National Information and Documentation Center (NIDOC)

a quinoid form structure during the un-doping process. In comparison to polyaniline, PoPDA consists of benzene rings and imine nitrogen or secondary amine atoms, similar to polyaniline polymer. The PoPDA polymer, on the other hand, has a distinct molecular structure [9,10].

In this work, poly (o-phenylenediamine) (PoPDA) has been synthesized using ammonium persulfate (APS) as an oxidizing agent of the o-phenylenediamine monomer. The synthesized PoPDA was doped by rGO nanosheets and ZnO nanoparticles and then mixed with PVA polymer. The PVA/PoPDA-rGO-ZnO nanocomposite was examined using XRD, SEM, FT-IR, capacitance data to investigate the structural and electrical properties and compared with the undoped PVA polymer. The aim of this work is to study the electrical properties of these films in order to use them in sensors and capacitors to store electrical charges.

## 2. Experimental

### 2.1. Materials

All materials and solutions used in this work were used as received without any further purification processes. All chemicals were purchased from Sigma Chemical Company.

### 2.2. Preparation Methods

#### 2.2.1. Preparation of Reduced Graphene Oxide nanopowder

Graphene oxide (GO) has been synthesized from pure graphite by using the modified Hummer method [11]. The obtained graphene oxide (GO) was reduced to yield the reduced graphene oxide (rGO) using hydrazine hydrate ( $N_2H_4 \cdot H_2O$ ) as in the following steps: 100 mg of graphene oxide was dispersed in (100 ml) of deionized water. The inhomogeneous aqueous solution of GO was transferred to the ultrasonic water bath, in order to disperse graphene oxide in the deionized water. Then, (1 ml) of hydrazine hydrate was added to the GO aqueous solution. The obtained mixture was condensed at 100 °C with stirring for 24 h. The reduced graphene oxide rGO was obtained as a black precipitated powder; the rGO powder was filtered and then washed several times with deionized water to remove the residual hydrazine traces. Then, the black powder dried at 80 °C for 24 h to obtain the final rGO product [12].

#### 2.2.2. Preparation of zinc oxide nanoparticles

The zinc oxide ZnO nanoparticles were made using a simple precipitation method in which

(0.2M) of zinc nitrate trihydrate ( $ZnO(NO_3)_3 \cdot 3H_2O$ ) and (0.4M) of sodium bicarbonate ( $NaHCO_3$ ) were dissolved separately in 100 ml of distilled water and stirred for half an hour to obtain homogeneous and clear solutions. The aqueous solution of sodium bicarbonate was added gradually to the aqueous solution of zinc nitrate with continuous mixing and at a temperature of 50 °C until the pH of the mixture reached 6.8, and then white precipitated particles were obtained from the reaction. The obtained zinc oxide particles were filtered and washed with distilled water several times to remove the bicarbonate residue and dried in the air for two hours at 80. The final powder is calcined for three hours at 400 °C under air to yield ZnO nanoparticles [13].

#### 2.2.3. Preparation of (rGO-ZnO) nanocomposite mixture

The GO-ZnO nanocomposite mixture was prepared by the following steps: 0.5 g of synthesized reduced graphene oxide rGO dispersed in 100 ml of deionized water. The rGO solution was well mixed using an ultrasonic mixer at room temperature of 25 °C for 1 h to obtain a homogeneous rGO solution. Thereafter, 0.5 g of synthesized zinc oxide ZnO nanorods was added gradually to the rGO solution with continuous stirring for 2 h, and then the mixture sonicated for 1 h in order to obtain homogeneous nanoparticles suspended in the solution. The resulting mixture was centrifuged to separate the nanoparticles and dried in an oven for 24 hours at 80 °C under air to produce the rGO-ZnO nanocomposite.

#### 2.2.4. Preparation of the ternary (rGO-ZnO-PoPDA) nanocomposite

The ternary rGO-ZnO-PoPDA nanocomposite was prepared by dispersing 0.5 g of the rGO-ZnO mixture in 50 ml of deionized water using an ultrasonic bath at room temperature of 25 °C for 1h.

Solution of 1.62 g of o-phenylenediamine monomer dissolved in 100 ml of 0.1 M of hydrochloric acid with constant stirring in a cold water bath. Then the two solutions were mixed under continuous stirring for 1 hour as the starting solution. Separately, an oxidizing agent solution was prepared by dissolving 6 g of ammonium persulfate (APS) in 100 ml of 0.1 M of hydrochloric acid in a cold water bath, and then gradually added to the starting solution under vigorous stirring for 24 h at room temperature (25 °C) until the precipitate was obtained. The final product was filtered and washed with distilled water and acetone

several times, then dried in an oven under air at 80 °C for 24 h to yield a ternary (rGO-ZnO-POPDA) nanocomposite [14,15].

### 2.2.5. Fabrication of PVA/rGO- ZnO-POPDA film

2. The PVA/rGO-ZnO-POPDA nanocomposite film was prepared by dissolving 2 g of PVA in 20 ml of hot distilled water with constant stirring at 60 °C to yield a homogeneous solution. Then, 0.1g of ternary rGO-ZnO-POPDA nanocomposite was dispersed in 5 mL of distilled water and gradually added to the PVA solution. The resulting mixture was continuously mixed for 1 hour at 50°C to obtain a homogeneous solution. The final solution was sonicated at room temperature (25 °C) for half an hour before the casting process on a glass substrate, then dried in an oven at 60°C under vacuum. The casted film was peeled off to yield the PVA/rGO-ZnO-POPDA nanocomposite film.

## 3. Result and Discussion

### 3.1. Structural Characterizations

#### 3.1.1. X-ray Diffraction (XRD)

The crystalline structure of the PVA/rGO-ZnO-PoPDA nanocomposite film was determined by using a (Shimadzu XRD-6000 powder) diffractometer, with radiation Cu K $\alpha$  and a scanning rate of 5° min<sup>-1</sup> to characterize the crystal structure type of the synthesized nanocomposite film. Figure 1 shows the typical x- ray diffraction spectrum of PVA/rGO-ZnO-PoPDA nanocomposite film in the range of 2 $\theta$  (15° to 80°). The XRD spectrum showed the formation of the crystalline phase of the PVA/rGO-ZnO-PoPDA nanocomposite. The obtained spectrum presents several characteristic peaks of rGO, ZnO and PoPDA phases. The detected peaks at (2 $\theta$  =24.9°) for (002) plane and (2 $\theta$  = 42.8°) for the (001) plane are attributed to the formation of reduced graphene oxide (rGO) corresponding with the obtained results by [16 ,17]. The peaks at (2 $\theta$  =31.8°, 34.5°, 36.8°, 47.7°) for (100) (002) (101) (102) planes respectively matches the characteristic peaks of zinc oxide (ZnO) with hexagonal crystal structure, space group (P63mc- no.186) according to (ICDD 01-070-2551), and agreed with [18,19 ,20 ,21]. Other several peaks located at (2 $\theta$  =8.53°, 9.52°, 11.15°, 17.05°, 18.77°, 21.63°, 22.67°, 25.65°, 27.66°, 29.28°, 34.21°, 38.21°, 40.44°, 41.71°) which referred to the formation of crystalline phase of PoPDA [22]. In addition, the characteristic peaks of graphite were observed at (2 $\theta$  = 26.4°, 54.6°) for (002) (004) planes [23].

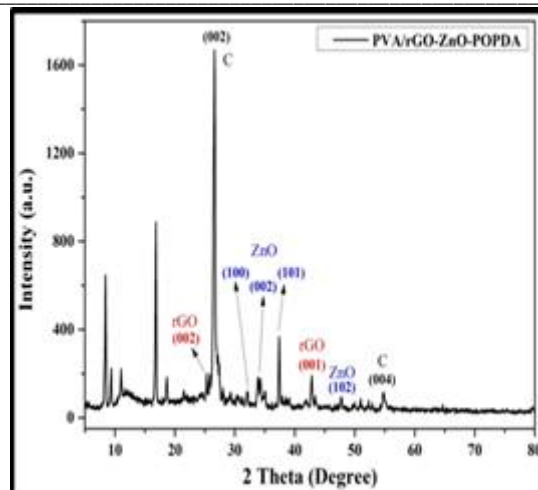


Figure 1. X-ray diffraction pattern of ternary rGO – ZnO-POPDA nanocomposite.

#### 3.1.2. Scanning Electron Microscopy (SEM)

Scanning electron microscopy SEM was used to investigate the morphologies of prepared samples. Figure 2(a, b, c) presents SEM morphology images of the prepared GO, rGO, ZnO respectively.

Figure 2a. shows that the graphene oxide GO has sheet-like graphene oxide nanostructures with a thickness of about (35.56 nm). It can be seen that the GO sheets are folded and rolled due to the presence of oxygen groups at the edges of the sheets; some agglomerations of more than one sheet can be observed. In addition, some wrinkled sheets and nanoparticles with a diameter of about (36.93 nm) appear on the GO surface as a result of the graphite oxidation process through the formation of fully oxidized graphene oxide [24]. The reduced graphene oxide rGO appeared as irregular oriented crumpled nanosheets with a thickness of about (20.32 nm) that was attributed to good exfoliation of prepared rGO sheets [25], as shown in fig. 2b. The morphology of prepared zinc oxide ZnO consists of a large number of crystalline ZnO nanoparticles with an average diameter of about (48.4 nm) stacked as curved and uniform ZnO nanosheets to form a flower-like ZnO structure. The ZnO nanosheets are arranged on a common central axis, as shown in fig. 2c.

SEM morphology images of pure PoPDA polymer and the PVA/rGO-ZnO-PoPDA ternary composite are shown in Figs. 3a, b. Figure 2a depicts the morphology nature of prepared PoPDA. The POPDA polymer has irregular shapes as short-micro rod structures with various dimensions and high surface areas, which can be attributed to PoPDA self-assembling via intermolecular – and electrostatic repulsion interactions [26,27]. SEM images indicated that the mixing of rGO

nanosheets, ZnO flower-like, and crystalline PoPDA polymer on PVA film led to the formation of crystalline nanorods with different lengths and diameters (204 nm), with perfectly smooth surfaces.

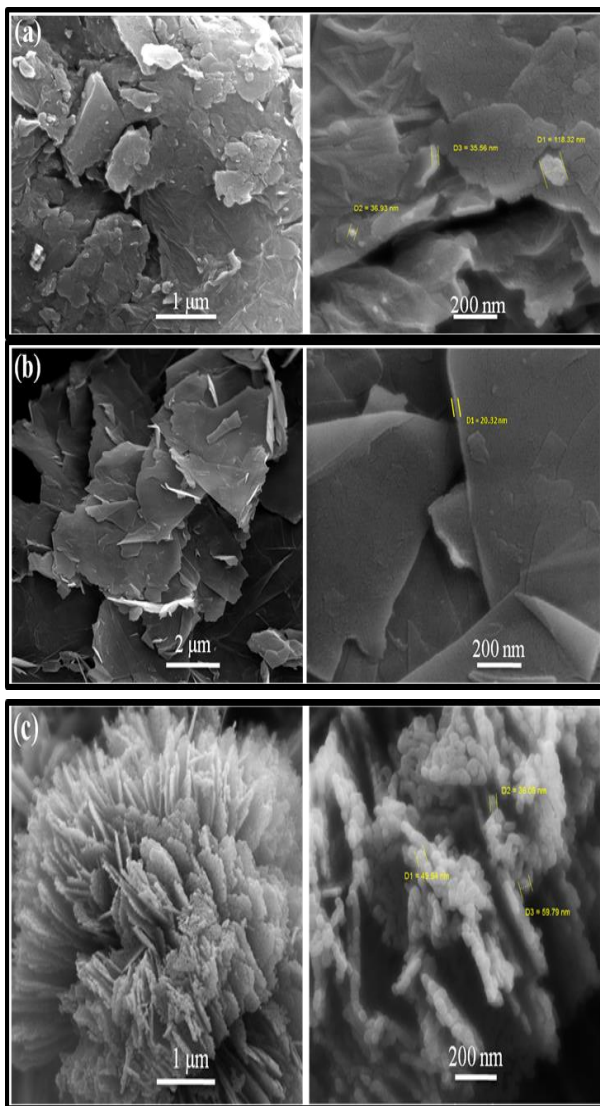


Figure 2. SEM morphology images of (a) Graphene oxide GO (b) Reduced graphene oxide rGO and (c) Zinc oxide ZnO nanopowders.

### 3.1.3. Fourier-transform Infrared (FTIR)

The Fourier-transform Infrared spectroscopy FTIR examination was carried out in order to identify the functional groups in the prepared ternary nanocomposite. Figure 4 presents the FTIR spectrum of ternary PVA/rGO-ZnO-PoPDA nanocomposite film. From the obtained spectrum, several characteristic bands were detected. The vibration bands located at 437 cm<sup>-1</sup> and 671 cm<sup>-1</sup>

are ascribed to the Zn-O bond (metal-oxygen) [28]. The vibration bands at 591 cm<sup>-1</sup> and 732 cm<sup>-1</sup> are attributed to the bending vibration of the C-H bond outside the plane of benzene units [12]. The two vibration bands at 852 cm<sup>-1</sup> and 3145 cm<sup>-1</sup> can be assigned to the rocking and stretching vibrations of the O-H bond, respectively, resulting from the water molecules adsorbed by the sample from the ambient [29]. The vibration band at 1226 cm<sup>-1</sup> indicated the presence of oxygen that contains the functional groups on the graphene nanosheets [30, 31].

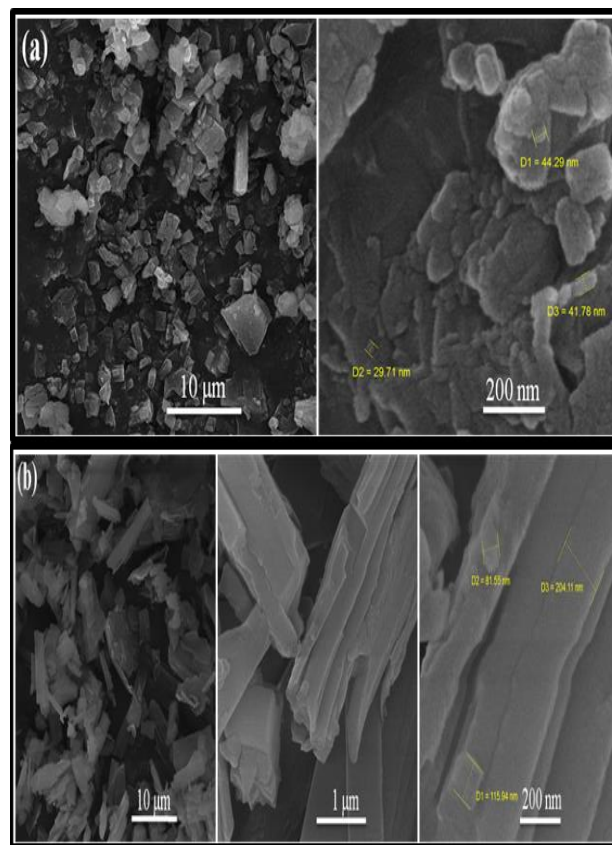


Figure 3. Pure PoPDA polymer (b) Ternary PVA/rGO-ZnO-POPDA nanocomposite

The band located at 1368 cm<sup>-1</sup> ascribed to the C-N stretching vibrations in the quinoid imine unit [8]. The characteristic band located at 1487 cm<sup>-1</sup> is ascribed to stretching vibrations of the C=C bond in the benzenoid ring [32]. The vibration band at 1149 cm<sup>-1</sup> can be attributed to the stretching vibrations of the C-O-C bond [33]. The vibration bands located at 1535 cm<sup>-1</sup> and 1629 cm<sup>-1</sup> are assigned to the C=C and C=N stretching vibrations respectively in the phenazine ring [8]. The stretching vibrations of the C-H bond are assigned to the two bands at 2780 cm<sup>-1</sup> and 2883 cm<sup>-1</sup> [34,35]. Finally, the

characteristic band located at 3315  $\text{cm}^{-1}$  can be attributed to the stretching vibrations of the N–H bond in the –NH– group [8]. The detected bands referred to the formation of the proposed ternary PVA/rGO-ZnO-PoPDA nanocomposite.

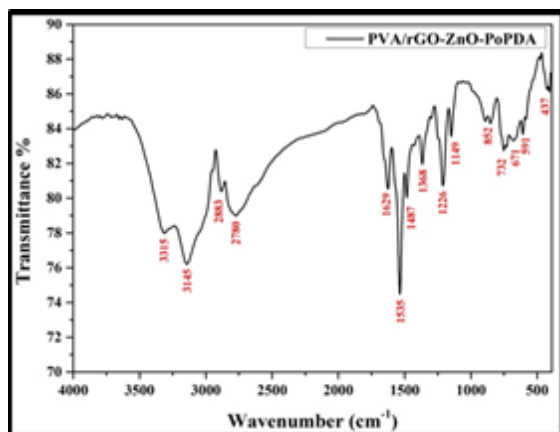


Figure4. FTIR spectrum of prepared ternary PVA/rGO-ZnO-PoPDA nanocomposite film.

### 3.2. Electrical Characterizations

#### 3.2.1. Dielectric Constant ( $\epsilon'$ )

The dielectric constant of pure PVA and PVA:POPAD-rGO-ZnO films was measured, within the frequency range (1MHz-5MHz) at room temperature (25°C). Figure 5 shows the dielectric constant ( $\epsilon'$ ) behavior as a function of frequency. The results indicated that the dielectric constant ( $\epsilon'$ ) values significantly decreased with increasing the frequency, as shown in table 1. The low dielectric constant values ascribed to the electric dipoles within the macromolecules are arranged in the same direction as the applied electric field at low frequencies, while at high-frequency values, the electric dipoles are unable to be arranged due to the rapid changes in the applied electric field, as well as due to the effects of polarization of the electrode [36, 37]. Therefore, at high frequencies, the periodic reversal of the electric field occurs very quickly, as there is no further ion diffusion in the direction of the electric field, which leads to reduced polarization resulting from charge accumulation, thus, lower values of the dielectric constant [38]. In fact, the initial dielectric constant has high values for polar materials and then decreases with frequency. The same behavior was observed in a number of polymers [39, 40].

The addition of prepared ternary (POPDA-rGO-ZnO) nanocomposite led to an increase in the dielectric constant ( $\epsilon'$ ) values of PVA film at all frequencies, which can be attributed to the inorganic nanoparticles filling the internal cavities which

separate two adjacent energy levels and reduce the voltage barrier, thus facilitating the transfer of ions between different levels within the structure of the PVA polymer film. In addition, the phase difference between the PVA film and the ternary nanocomposite leads to the creation of interfaces within the PVA film structure, thus increasing the polarity (i.e., a high number of dipoles per unit volume). The obtained results indicate the effect of the good interaction between the ternary nanocomposite and the PVA polymer, which may modify the movement of the polymeric chains, leading to enhanced polarization of the prepared material [41, 42, 43].

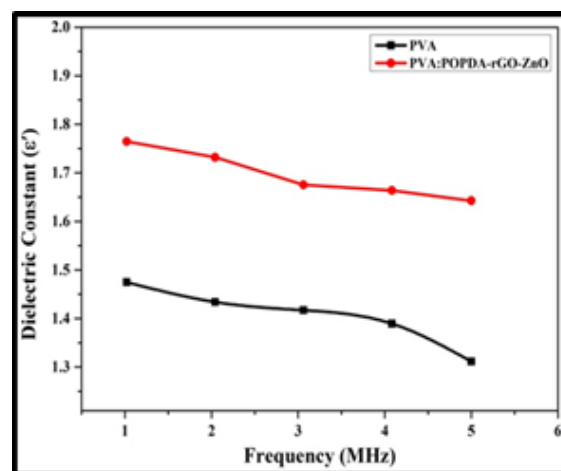


Figure5. Dielectric constant vs. frequency of pure PVA and PVA/rGO-ZnO-PoPDA nanocomposite films.

#### 3.2.2. Dissipation Factor ( $\epsilon''$ )

The dissipation factor (loss factor) is a measure of the energy loss ratio to the total energy passing through the insulator. The energy dissipated by the insulator is proportional to the loss factor. The study of dissipation factors related to polymeric composite applications. The dissipation factor ( $\epsilon''$ ) exam was carried out of pure PVA and PVA:POPAD-rGO-ZnO films within the frequency range (1MHz-5MHz) at room temperature (25°C). Figure 6 presents the dissipation factor of prepared films as a function of frequency. It is observed that the values of the dissipation factor ( $\epsilon''$ ) of pure PVA and PVA:POPAD-rGO-ZnO films decrease with frequency, as shown in table 1, due to the impediment of charge movement and dissipation of energy with the increase of the applied electric field frequency. Thus, electrical dipoles require higher energy in order to achieve a relaxation state [44]. The results revealed that the adding of ternary

nanocomposite led to a significant decrease in the dissipation factor values at the same frequency. The polymeric nanocomposite (PVA/POPDA-rGO-ZnO) recorded the lowest values of dissipation factor as a result of increasing the charge carrier number and facilitating the charge movement when adding the ternary nanocomposite, thus reducing the dissipated energy [27].

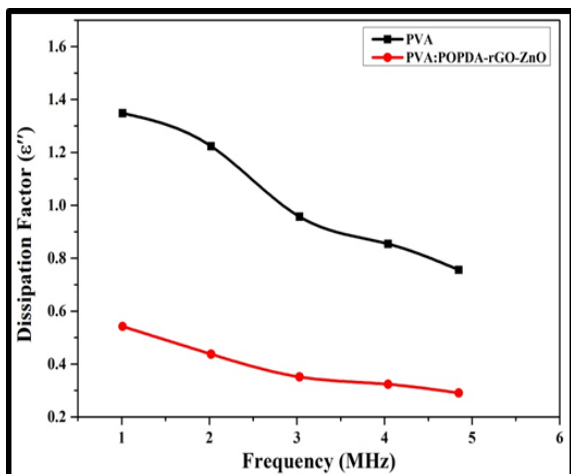


Figure 6. Dissipation factor vs. frequency of pure PVA and PVA/rGO-ZnO-PoPDA nanocomposite films.

### 3.2.3 A.C Electrical Conductivity ( $\sigma_{a.c}$ )

The A.C. electrical conductivity ( $\sigma_{a.c}$ ) was carried out on pure PVA and PVA: POPDA-rGO-ZnO films, within the frequency range (1MHz - 5MHz) at room temperature (25°C). Figure 7 presents the A.C. electrical conductivity ( $\sigma_{a.c}$ ) of prepared films as a function of frequency. The results showed increasing the AC electrical conductivity ( $\sigma_{a.c}$ ) values of all prepared films with increasing frequency, as shown in table 1. It can be explained by the fact that the increase in applied electric field frequency leads to high polarization within the material, and jumping the charge carriers between the levels, i.e. the sudden transfer of charge carriers from one position to another neighboring position by increasing the frequency. The transition process involves both jumping through the voltage barrier and quantum mechanical tunneling. Furthermore, increasing AC electrical conductivity with frequency is a characteristic of polymeric and semiconductor materials [45,46]. The alternating electrical conductivity of insulating materials is highly dependent on the frequency because it is the amount of energy lost when exposed to an alternating electric field. The lost energy is in the form of heat resulting from the vibration of electric

dipoles and charges during the changing of the alternating electric field [47].

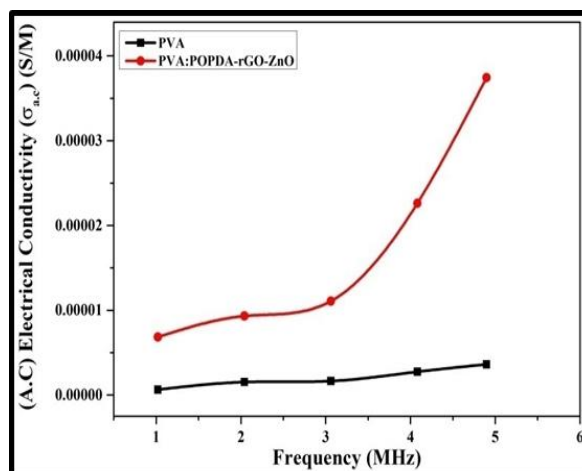


Figure 7. A.C electrical conductivity vs. frequency of pure PVA and PVA/rGO-ZnO-PoPDA nanocomposite films.

From figure 7, it is observed that the values of AC electrical conductivity are increased by adding the ternary (PoPDA-rGO-ZnO) nanocomposite. The ternary nanocomposite can build conductive paths within the structure of the composite material, which leads to increasing the alternating electrical conductivity ( $\sigma_{a.c}$ ) values and reducing the insulator resistance [31].

The obtained results showed that the ternary PVA/PoPDA-rGO-ZnO nanocomposite has good electrical properties which can be attributed to the presence of reduced graphene oxide rGO nanosheets, where the rGO nanosheets are well dispersed within the polymer to store a large number of electric charges at the interfaces with the polymer, the adjacent pair of conductive rGO nanosheets separated by the polymer film can act as a nanocapacitor thus, the composite material consists of a network of nanocapacitors, to improve the electrical properties [49, 50].

### Recommendation

This study can be used in the future through:

- 1- The use of polymeric nanocomposites to measure its ability to store hydrogen and to remove heavy metals from their solutions.
- 2- The use of prepared materials in lithium batteries, fuel cells, and storage of carbon dioxide and other useful gases.
- 3- These new materials prepared are applied in the sensors of some gases such as ammonia and carbon dioxide.

Table 1 Dielectric constant, dissipation factor and A.C. electrical conductivity values of prepared films at different frequency.

Frequency (MHz)	Dielectric Constant ( $\epsilon'$ )		Dissipation Factor ( $\epsilon''$ )		A.C Electrical Conductivity (S/m)* $10^{-5}$	
	PVA	PVA:POPDA-rGO-ZnO	PVA	PVA:POPDA-rGO-ZnO	PVA	PVA:POPDA-rGO-ZnO
1	1.47482	1.7645	1.34803	0.54226	0.06397	0.68492
2	1.43392	1.73185	1.22307	0.4374	0.15344	0.93198
3	1.41706	1.67516	0.95675	0.35146	0.16523	1.10823
4	1.38944	1.66374	0.85418	0.32372	0.27525	2.26307
5	1.31152	1.64251	0.75582	0.29054	0.36204	3.74425

#### 4. Conclusions

In summary, graphene oxide GO like-nanosheets, rGO nanosheets, zinc oxide ZnO like-flower, and ternary PVA/PoPDA-rGO-ZnO nanocomposite have been successfully prepared. The XRD, SEM, and FTIR tests proved the formation of the crystalline phase of the ternary PVA/PoPDA-rGO-ZnO nanocomposite. The obtained results revealed that the addition of ternary PoPDA-rGO-ZnO nanocomposite led to an improvement in the electrical properties of the PVA polymer. The prepared PVA/PoPDA-rGO-ZnO nanocomposite exhibits good electrical properties; the highest A.C. electrical conductivity ( $\sigma_{a.c}$ ) ( $3.74 \times 10^{-5}$  S/m) was recorded at a high frequency of (5 MHz). The A.C. electrical conductivity increased with an increase in the applied electric field frequency. The highest dielectric constant ( $\epsilon'$ ) (1.7645) at the frequency of (1 MHz) and the lowest dissipation factor ( $\epsilon''$ ) (0.29054) at the frequency of (5 MHz) achieved by the crystalline PVA/PoPDA-rGO-ZnO nanocomposite. The ( $\epsilon'$ ) and ( $\epsilon''$ ) values decreased with the frequency. This improvement is ascribed to the presence of rGO nanosheets which efficiently improve the ability to store a large number of electric charges at the interfaces with the polymer, as a network of nanocapacitors to improve the electrical performance. The prepared PVA/PoPDA-rGO-ZnO nanocomposite is a good candidate for electrical applications as capacitors and sensors.

#### 5. References

[1] Su, P. G., & Lu, Z. M. (2015). Flexibility and electrical and humidity-sensing properties of diamine-functionalized graphene oxide films.

Sensors and Actuators B: Chemical, 211, 157-163.

- [2] Sivakumar, S., Mala, N. A., Bato, K. M., & Raslan, E. H. (2021). Efficient, highly stable Zn<sup>2+</sup> doped NiO nanoparticles with enhanced magnetic and supercapacitor applications. *Materials Technology*, 1-13.
- [3] Chauhan, A., Verma, R., Kumari, S., Sharma, A., Shandilya, P., Li, X., ... & Kumar, R. (2020). Photocatalytic dye degradation and antimicrobial activities of Pure and Ag-doped ZnO using Cannabis sativa leaf extract. *Scientific reports*, 10(1), 1-16.
- [4] Dhiman, P., Chand, J., Kumar, A., Kotnala, R. K., Bato, K. M., & Singh, M. (2013). Synthesis and characterization of novel Fe@ZnO nanosystem. *Journal of alloys and compounds*, 578, 235-241.
- [5] Cha, J. R., & Gong, M. S. (2013). Preparation of epoxy/polyelectrolyte IPNs for flexible polyimide-based humidity sensors and their properties. *Sensors and Actuators B: Chemical*, 178, 656-662.
- [6] Ho, T. A., Jun, T. S., & Kim, Y. S. (2013). Material and NH<sub>3</sub>-sensing properties of polypyrrole-coated tungsten oxide nanofibers. *Sensors and Actuators B: Chemical*, 185, 523-529.
- [7] Olgun, U., & Gülfe, M. (2014). Doping of poly(o-phenylenediamine): spectroscopy, voltammetry, conductivity and band gap energy. *Reactive and Functional Polymers*, 77, 23-29.
- [8] Majeed, A. H., Hussain, D. H., Al-Tikrity, E. T. B., & Alheety, M. A. (2020). Poly(o-Phenylenediamine-GO-TiO<sub>2</sub>) nanocomposite: modulation, characterization and thermodynamic calculations on its H<sub>2</sub> storage

- capacity. *Chemical Data Collections*, 28, 100450.
- [9] Lu, X., Mao, H., Chao, D., Zhao, X., Zhang, W., & Wei, Y. (2007). Preparation and characterization of poly (o-phenylenediamine) microrods using ferric chloride as an oxidant. *Materials Letters*, 61(6), 1400-1403.
- [10] Pisarevskaya, E. Y., Ovsyannikova, E. V., & Alpatova, N. M. (2004). Two-layered poly-o-phenylenediamine/polyaniline composite: Electrosynthesis and spectroelectrochemical properties. *Russian Journal of Electrochemistry*, 40(9), 969-976.
- [11] Zaaba, N. I., Foo, K. L., Hashim, U., Tan, S. J., Liu, W. W., & Voon, C. H. (2017). Synthesis of graphene oxide using modified hummers method: solvent influence. *Procedia engineering*, 184, 469-477.
- [12] Zhou, S., Wu, Y., Zhao, W., Yu, J., Jiang, F., Wu, Y., & Ma, L. (2019). Designing reduced graphene oxide/zinc rich epoxy composite coatings for improving the anticorrosion performance of carbon steel substrate. *Materials & Design*, 169, 107694.
- [13] Mubarak, T. H., Hassan, K. H., & Abbas, Z. M. A. (2013). Using X-ray diffraction and scanning electron microscope to study zinc oxide nanoparticles prepared by wet chemical method. In *Advanced Materials Research* (Vol. 685, pp. 119-122). Trans Tech Publications Ltd.
- [14] Samanta, S., Roy, P., & Kar, P. (2016). Structure and properties of conducting poly (o-phenylenediamine) synthesized in different inorganic acid medium. *Macromolecular Research*, 24(4), 342-349.
- [15] Deng, W., Zhang, Y., Tan, Y., & Ma, M. (2017). Three-dimensional nitrogen-doped graphene derived from poly-o-phenylenediamine for high-performance supercapacitors. *Journal of Electroanalytical Chemistry*, 787, 103-109.
- [16] Low, F. W., Lai, C. W., & Abd Hamid, S. B. (2015). Easy preparation of ultrathin reduced graphene oxide sheets at a high stirring speed. *Ceramics International*, 41(4), 5798-5806.
- [17] Thakur, S., & Karak, N. (2012). Green reduction of graphene oxide by aqueous phytoextracts. *Carbon*, 50(14), 5331-5339.
- [18] Al-Douri, Y., Gherab, K., Batoo, K. M., & Raslan, E. H. (2020). Detecting the DNA of dengue serotype 2 using aluminium nanoparticle doped zinc oxide nanostructure: synthesis, analysis and characterization. *Journal of Materials Research and Technology*, 9(3), 5515-5523.
- [19] Balakrishnan, G., Sinha, V., Peethala, Y. P., Kumar, M., Nimal, R. J., Hussain, J. H., ... & Raslan, E. H. (2020). Structural and optical properties of ZnO thin film prepared by sol-gel spin coating. *Materials Science Poland*, 38.
- [20] Wasly, H. S., Abd El-Sadek, M. S., & Batoo, K. M. (2019). Novel synthesis, structural, optical properties and antibacterial activity of ZnO nanoparticles. *Materials Research Express*, 6(5), 055003.
- [21] Dhiman, P., Batoo, K. M., Kotnala, R. K., Chand, J., & Singh, M. (2013). Room temperature ferromagnetism and structural characterization of Fe, Ni co-doped ZnO nanocrystals. *Applied surface science*, 287, 287-292.
- [22] Zoromba, M. S., Abdel-Aziz, M. H., Bassyouni, M., Bahaiham, H., & Al-Hossainy, A. F. (2018). Poly (o-phenylenediamine) thin film for organic solar cell applications. *Journal of Solid State Electrochemistry*, 22(12), 3673-3687.
- [23] Low, F. W., Lai, C. W., & Abd Hamid, S. B. (2015). Easy preparation of ultrathin reduced graphene oxide sheets at a high stirring speed. *Ceramics International*, 41(4), 5798-5806.
- [24] Dubey, S. P., Nguyen, T. T., Kwon, Y. N., & Lee, C. (2015). Synthesis and characterization of metal-doped reduced graphene oxide composites, and their application in removal of *Escherichia coli*, arsenic and 4-nitrophenol. *Journal of Industrial and Engineering Chemistry*, 29, 282-288.
- [25] Stankovich, S., Dikin, D. A., Piner, R. D., Kohlhaas, K. A., Kleinhammes, A., Jia, Y., ... & Ruoff, R. S. (2007). Synthesis of graphene-based nanosheets via chemical reduction of exfoliated graphite oxide. *carbon*, 45(7), 1558-1565.
- [26] Lu, X., Mao, H., Chao, D., Zhao, X., Zhang, W., & Wei, Y. (2007). Preparation and characterization of poly (o-phenylenediamine) microrods using ferric chloride as an oxidant. *Materials Letters*, 61(6), 1400-1403.
- [27] Sun, X., Dong, S., & Wang, E. (2005). Formation of o-phenylenediamine oligomers and their self-assembly into one-dimensional structures in aqueous medium. *Macromolecular rapid communications*, 26(18), 1504-1508.
- [28] Suresh, J., Pradheesh, G., Alexramani, V., Sundrarajan, M., & Hong, S. I. (2018). Green synthesis and characterization of zinc oxide

- nanoparticle using insulin plant (*Costus pictus* D. Don) and investigation of its antimicrobial as well as anticancer activities. *Advances in Natural Sciences: Nanoscience and Nanotechnology*, 9(1), 015008.
- [29] Headrick, J. M., Diken, E. G., Walters, R. S., Hammer, N. I., Christie, R. A., Cui, J., ... & Jordan, K. D. (2005). Spectral signatures of hydrated proton vibrations in water clusters. *Science*, 308(5729), 1765-1769.
- [30] Bourlinos, A. B., Gournis, D., Petridis, D., Szabó, T., Szeri, A., & Dékány, I. (2003). Graphite oxide: chemical reduction to graphite and surface modification with primary aliphatic amines and amino acids. *Langmuir*, 19(15), 6050-6055.
- [31] Xu, C., Wang, X., & Zhu, J. (2008). Graphene-metal particle nanocomposites. *The Journal of Physical Chemistry C*, 112(50), 19841-19845.
- [32] Cong, H. P., Ren, X. C., Wang, P., & Yu, S. H. (2013). Flexible graphene-polyaniline composite paper for high-performance supercapacitor. *Energy & Environmental Science*, 6(4), 1185-1191.
- [33] Copikova, J., Cerna, M., Novotna, M., Kaasova, J. I. T. K. A., & Synytsya, A. (2001). Application of FT-IR spectroscopy in detection of food hydrocolloids confectionery jellies and in food supplements. *Czech Journal of Food Sciences*, 19(2), 51-56.
- [34] Mitchell, C. J., Yang, G. R., & Senkevich, J. J. (2006). Adhesion aspects of poly (p-xylylene) to SiO<sub>2</sub> surfaces using  $\gamma$ -methacryloxypropyltrimethoxysilane as an adhesion promoter. *Journal of adhesion science and technology*, 20(14), 1637-1647.
- [35] Drabczyk, A., Kudłacik-Kramarczyk, S., Głab, M., Kędzierska, M., Jaromin, A., Mierzwiński, D., & Tylińczak, B. (2020). Physicochemical investigations of chitosan-based hydrogels containing Aloe Vera designed for biomedical use. *Materials*, 13(14), 3073.
- [36] Ramesh, S., Yahana, A. H., & Arof, A. K. (2002). *Solid State Ionics* 152-153: 291. doi: 10.1016/S0167-2738(02), 00311-9.
- [37] Tareev, B., & Tareev, B. M. (1979). *Physics of Dielectric Materials*, Mir Publ.
- [38] Campbell, J. A., Goodwin, A. A., & Simon, G. P. (2001). Dielectric relaxation studies of miscible polycarbonate/polyester blends. *Polymer*, 42(10), 4731-4741.
- [39] Pillai, P. K. C., Khurana, P., & Tripathi, A. (1986). Dielectric studies of poly (methyl methacrylate)/polystyrene double layer system. *Journal of materials science letters*, 5(6), 629-632.
- [40] Rao, R. V., & Shridhar, M. H. (2002). Interfacial polarization in poly (4-vinyl pyridine)/NiPc/I2 composite. *Materials letters*, 55(1-2), 34-40.
- [41] Psarras, G. C., Gatos, K. G., Karahaliou, P. K., Georga, S. N., Krontiras, C. A., & Karger-Kocsis, J. (2007). Relaxation phenomena in rubber/layered silicate nanocomposites. *Express Polym Lett*, 1(12), 837-845.
- [42] Fan, B., Liu, Y., He, D., & Bai, J. (2017). Influences of thermal treatment on the dielectric performances of polystyrene composites reinforced by graphene nanoplatelets. *Materials*, 10(7), 838.
- [43] Hashim, A., Agool, I. R., & Kadhim, K. J. (2018). Novel of (polymer blend-Fe<sub>3</sub>O<sub>4</sub>) magnetic nanocomposites: preparation and characterization for thermal energy storage and release, gamma ray shielding, antibacterial activity and humidity sensors applications. *Journal of Materials Science: Materials in Electronics*, 29(12), 10369-10394.
- [44] Foulger, S. H. (1999). Electrical properties of composites in the vicinity of the percolation threshold. *Journal of Applied Polymer Science*, 72(12), 1573-1582.
- [45] Divya, R., Meena, M., Mahadevan, C. K., & Padma, C. M. (2014). Investigation on CuO dispersed PVA polymer films. *Journal of Engineering Research and Applications*, 4(5), 1-7.
- [46] Gherab, K., Al-Douri, Y., Hashim, U., Ameri, M., Bouhemadou, A., Batoo, K. M., ... & Raslan, E. H. (2020). Fabrication and characterizations of Al nanoparticles doped ZnO nanostructures-based integrated electrochemical biosensor. *Journal of Materials Research and Technology*, 9(1), 857-867.
- [47] Popielarz, R., Chiang, C. K., Nozaki, R., & Obrzut, J. (2001). Dielectric properties of polymer/ferroelectric ceramic composites from 100 Hz to 10 GHz. *Macromolecules*, 34(17), 5910-5915.
- [48] Wang, D., Zhang, X., Zha, J. W., Zhao, J., Dang, Z. M., & Hu, G. H. (2013). Dielectric properties of reduced graphene oxide/polypropylene composites with ultralow percolation threshold. *Polymer*, 54(7), 1916-1922.
- [49] Yousefi, N., Sun, X., Lin, X., Shen, X., Jia, J., Zhang, B., ... & Kim, J. K. (2014). Highly

aligned graphene/polymer nanocomposites with excellent dielectric properties for high-performance electromagnetic interference shielding. *Advanced Materials*, 26(31), 5480-5487.

- [50]Zhou, W., &Cai, J. (2012). Mechanical and dielectric properties of epoxy resin modified using reactive liquid rubber (HTPB). *Journal of applied polymer science*, 124(5), 4346-4351.